European Journal of Clinical Pharmacy
Print ISSN: 2385-409X **Online ISSN**: 3105-0409
Website: https://farmclin.com/

Original Research Article

Green Synthesis and Characterization of ZnO Nanoparticles Using Trichoderma harzianum for Antimicrobial Activity against MDR Pathogens

Article History:

Name of Author:

Nain Taara Bukhari[1], Tawab Ali[2], Fazal Hanan[3], Iqbal Nisa[4], Ajet Kumar[5], Nazir Ahmed shah[6], Sudhair Abbas Bangash[7], Saher sami[8], Emaan Mansoor[9], Ezza Mansoor[10], Efrah Mansoor[11], Afsheen Mansoor[12]

Affiliation: *[1]Department of Microbiology, Bahria university of health Science, Karachi Campus*

[2]Centre for Biotechnology and Microbiology (CBM), University of swat, Pakistan.

[3]Department of Pathology (Microbiology) Saidu Group of Teaching Hospital/ Saidu Medical Collage Swat.

[4]Department of Microbiology, Women University swabi, Pakistan

[5]Department of Pharmacology Ghulam Muhammad Mahar Medical College Sukkur

[6]Department of pharmacology Ghulam Muhammad Mahar Medical College sukkur

[7]Faculty of Life Sciences, Department of Pharmacy Sarhad University of science and information technology, Peshawar

[8]Department of organic chemistry Urdu Federal University, Karachi Pakistan

[9,10,11] Islamic International Dental college, Riphah International University, Islamabad

[12]Department of Dental material Sciences, School of Dentistry, Shaheed Zulfiqar Ali Bhutto medical University, Islamabad.

[12]Department of Microbiology and Nanotechnology, Quaid-i-Azam

Abstract: The increasing prevalence of multidrug-resistant (MDR) bacterial infections has necessitated the development of alternative antimicrobial agents. In this study, zinc oxide nanoparticles (ZnO NPs) were synthesized using the fungal strain Trichoderma harzianum through a green, eco-friendly route. The biosynthesized ZnO NPs were characterized using UV-Vis spectroscopy, Fourier-transform infrared spectroscopy (FTIR), X-ray diffraction (XRD), and scanning electron microscopy (SEM), confirming their hexagonal wurtzite structure, functional group composition, and diverse nanostructural morphologies. The optical bandgap was observed at ~375 nm, indicating strong UV absorption, while FTIR confirmed the presence of Zn–O bonds and surface functional groups. SEM analysis revealed size variation from nanoscale particles to microstructured sheets, reflecting morphological diversity. The antimicrobial efficacy of ZnO NPs was evaluated against five clinically significant MDR bacterial strains: Escherichia coli, Staphylococcus aureus, Pseudomonas aeruginosa, Klebsiella pneumoniae, and Salmonella typhi. Disk diffusion assays demonstrated dose-dependent inhibition, with maximum activity observed at 200 µg/mL. The minimum inhibitory concentration (MIC) ranged from 12.5 µg/mL (E. coli) to 50 µg/mL (P. aeruginosa), while MBC values confirmed bactericidal effects with consistent MIC/MBC ratios of 0.5. ZnO NPs showed high antibacterial potency, particularly against E. coli and K. pneumoniae, and remained stable across different pH conditions for most strains. These findings highlight the potential of T. harzianum-mediated ZnO nanoparticles as effective and sustainable antimicrobial agents against MDR pathogens, offering promising applications in biomedical fields such as infection control, wound healing, and antimicrobial coatings.

Keywords: Antimicrobial resistance; Urinary tract infection; Uropathogens; Antibiotic susceptibility; Bacterial isolates; Clinical microbiology; Public health.

How to Cite: N.T. Bukhari, T. Ali, F. Hanan, I. Nisa, A. Kumar, N.A. Shah, S.A. Bangash, S. Sami, E. Mansoor, E. Mansoor, E. Mansoor, A. Mansoor.Green Synthesis and Characterization of ZnO Nanoparticles Using Trichoderma harzianum for Antimicrobial Activity against MDR Pathogens. *European Journal of Clinical Pharmacy*. 2025;7(1):3224-3237.

University, Islamabad.

Corresponding Author:
nisayam55@gmail.com

***Received**:* 04-11-2025
***Revised**:* 18-11-2025
***Accepted**:* 09-12-2025
***Published**:* 30-12-2025

INTRODUCTION

Nanotechnology has emerged as a transformative discipline with diverse applications in medicine, agriculture, energy, and environmental sciences (Ali Syed et al., 2024; S. Khan et al., 2023; Shobha et al., 2023). Among various nanomaterials, zinc oxide nanoparticles (ZnO NPs) have garnered significant attention due to their distinctive physicochemical properties, including high surface-area-to-volume ratio, optical transparency, chemical stability, and potent antimicrobial activity (Laraib et al., 2023; Shah et al., 2023). These characteristics make ZnO NPs highly desirable for biomedical applications, drug delivery systems, biosensors, and antimicrobial coatings (Khalil et al., 2022; Shobha et al., 2020). However, conventional synthesis methods, such as chemical precipitation, sol-gel, and hydrothermal techniques, often involve the use of hazardous chemicals, high energy consumption, and environmentally detrimental byproducts, raising concerns over sustainability and safety (T. Kaur, Bala, Kumar, & Vyas, 2022; Zaki et al., 2021). Consequently, the development of eco-friendly and cost-effective synthesis routes has become a priority in nanoscience research. In recent years, biological approaches, particularly fungal-mediated synthesis of nanoparticles, have gained prominence as sustainable alternatives to conventional methods. Fungi possess the inherent ability to synthesize nanoparticles through the secretion of extracellular enzymes, proteins, and metabolites, which act as reducing and stabilizing agents (Arya et al., 2021; Konappa et al., 2021). Among various fungal species, *Trichoderma harzianum*, a well-established biocontrol agent and plant growth promoter, has demonstrated remarkable potential in nanoparticle biosynthesis. *T. harzianum* produces an array of bioactive compounds, including enzymes, flavonoids, and alkaloids, which not only facilitate the synthesis of stable ZnO NPs but also enhance their antimicrobial properties (Shams, Helaly, Algeblawi, & Awad-Allah, 2023). Given its adaptability and prolific secretion of biomolecules, *T. harzianum* serves as an excellent biological factory for the green synthesis of ZnO nanoparticles. One of the critical applications of ZnO NPs lies in their **antimicrobial potential against multidrug-resistant (MDR) pathogens**, which have become a significant global health threat (El-Ashmony et al., 2022; Nandhini, Karthikeyan, & Rajeshkumar, 2024). According to the **World Health Organization (WHO),** antibiotic resistance contributes to over **700,000 deaths annually**, and this number is projected to rise to **10 million deaths per year by 2050** if no effective solutions are developed. MDR bacteria, including *Escherichia coli*, *Staphylococcus aureus*, *Klebsiella pneumoniae*, and *Pseudomonas aeruginosa*, are responsible for a large proportion of hospital-acquired infections, with mortality rates exceeding **30% in critical cases (Trzcińska-Wencel, Wypij, Terzyk, Rai, & Golińska, 2023)**. ZnO NPs have demonstrated strong antibacterial properties due to their ability to generate **reactive oxygen species (ROS), disrupt bacterial membranes, and interfere with cellular metabolism.** The green synthesis of ZnO nanoparticles using *T. harzianum* offers several advantages over conventional synthesis methods (El-Sawaf, El-Moslamy, Kamoun, & Hossain, 2024; S. A. Khan, Noreen, Kanwal, Iqbal, & Hussain, 2018). It eliminates the need for toxic chemicals, reduces environmental pollution, and enhances the biocompatibility of the nanoparticles. Moreover, fungal-derived biomolecules play a crucial role in modulating the size, morphology, and stability of ZnO NPs, which directly influence their antimicrobial efficacy (Akbar et al., 2020; Jabber & Hussein, 2019). The synergistic action of ZnO nanoparticles and bioactive metabolites secreted by *T. harzianum* may further enhance their antibacterial potential against MDR pathogens. Thus, exploring biogenic ZnO nanoparticles as novel antimicrobial agents could provide a sustainable and effective

solution to combat antibiotic-resistant bacterial infections (S. A. Khan, Shahid, & Lee, 2020; Rana et al., 2023; Youssef, Ismail, Fouad, & Mohamed, 2024). This study aims to synthesize and characterize ZnO nanoparticles using *Trichoderma harzianum* and evaluate their antimicrobial efficacy against MDR bacterial pathogens. The synthesized ZnO NPs will be subjected to various physicochemical characterization techniques, including UV-Vis spectroscopy, Fourier-transform infrared spectroscopy (FTIR), X-ray diffraction (XRD), and scanning electron microscopy (SEM), to determine their structural, morphological, and optical properties. Furthermore, the antimicrobial activity of ZnO NPs will be systematically assessed against clinically relevant MDR bacterial strains to elucidate their potential as an alternative antimicrobial agent.

2. Materials and Methods

2.1 Materials

The materials used in this study included zinc nitrate hexahydrate ($Zn(NO_3)_2{\cdot}6H_2O$), which was of analytical grade and purchased from a certified chemical supplier. *Trichoderma harzianum* was obtained from a microbial culture collection for the green synthesis of ZnO nanoparticles. Nutrient Agar (NA) and Mueller-Hinton Agar (MHA) were used for bacterial culture growth and antimicrobial activity assays. Clinical isolates of multidrug-resistant (MDR) bacterial strains, including *Escherichia coli, Staphylococcus aureus, Klebsiella pneumoniae*, and *Pseudomonas aeruginosa*, were obtained from a medical microbiology laboratory. Distilled water was used in all solution preparations and washing procedures to ensure purity and prevent contamination (Sarkar et al., 2024; Sun, Li, & Le, 2018).

2.2 Green Synthesis of ZnO Nanoparticles Using Trichoderma harzianum

2.2.1 Cultivation of *Trichoderma harzianum*

Trichoderma harzianum was initially cultured on Potato Dextrose Agar (PDA) plates and incubated at 28°C for five days to allow fungal growth. To prepare the fungal biomass for ZnO NP synthesis, five mycelial discs (each 5 mm in diameter) were inoculated into 100 mL of Potato Dextrose Broth (PDB) and incubated at 28°C on a rotary shaker at 150 rpm for seven days (Rizwana, Bokahri, Alfarhan, Aldehaish, & Alsaggabi, 2022). After the incubation period, the fungal biomass was separated by filtration using Whatman No.1 filter paper and washed thoroughly with distilled water to remove residual media components.

2.2.2 Preparation of Fungal Extract

The harvested fungal biomass was then transferred into 100 mL of distilled water and boiled at 60°C for 30 minutes to extract bioactive metabolites responsible for nanoparticle synthesis. The mixture was filtered using Whatman No.1 filter paper to obtain a clear fungal filtrate, which was used as a reducing and stabilizing agent in ZnO NP synthesis (AMRINDER KAuR, KAuR, Kalia, & SINgH, 2016).

2.2.3 Synthesis of ZnO Nanoparticles

For nanoparticle synthesis, 50 mL of fungal filtrate was mixed with 50 mL of 0.1 M zinc nitrate ($Zn(NO_3)_2{\cdot}6H_2O$) solution under continuous stirring at room temperature (25°C) for 24 hours. The reaction mixture was incubated at 60°C for 12 hours to facilitate the formation of ZnO NPs. After incubation, the formed nanoparticles were separated by centrifugation at 10,000 rpm for 15 minutes and washed three times with distilled water to remove any unreacted residues. The obtained ZnO NPs were dried at 100°C for five hours and further calcinated at 400°C for two hours in a muffle furnace to improve crystallinity. The final ZnO NP powder was collected and stored in an airtight container for further characterization and antimicrobial testing (Castro-Longoria, 2022; Dikshit et al., 2021).

2.3 Characterization of ZnO Nanoparticles

The synthesized ZnO NPs were characterized using various analytical techniques to determine their structural, morphological, and functional properties. UV-Vis spectroscopy was performed to analyze the optical properties of ZnO NPs within the wavelength range of 200–800 nm. X-ray diffraction (XRD) analysis was conducted using Cu-Kα radiation (λ = 1.5406 Å) to determine the crystalline phase and structural properties of the nanoparticles in the 2θ range of 10°–80°. Fourier-transform infrared spectroscopy (FTIR) was used to identify functional groups present in ZnO NPs, with spectra recorded in the range of 400–4000 cm^{-1}. Scanning electron microscopy (SEM) was performed to examine the morphology, shape, and size distribution of ZnO NPs under an accelerating voltage of 10–20 kV. Additionally, energy dispersive X-ray spectroscopy (EDX) was used to confirm the elemental composition and purity of the synthesized ZnO NPs (Guilger-Casagrande, Germano-Costa, Pasquoto-Stigliani, Fraceto, & Lima, 2019; Rao, 2023).

2.4 Antimicrobial Activity of ZnO Nanoparticles

2.4.1 Preparation of Bacterial Cultures

The antimicrobial activity of ZnO NPs was tested against MDR bacterial strains, including *E. coli, S. aureus, K. pneumoniae*, *P. aeruginosa and S.typhi* . These bacterial strains were cultured in nutrient broth and incubated at 37°C for 18 hours. Before antimicrobial assays, bacterial suspensions were adjusted to match the 0.5 McFarland standard, corresponding to

approximately 1.5 × 10^8 CFU/mL (F. Khan et al., 2022).

2.4.2 Disk Diffusion Method

To assess the antimicrobial efficacy of ZnO NPs, the disk diffusion method was employed. Freshly prepared Mueller-Hinton Agar (MHA) plates were inoculated with bacterial suspensions using a sterile cotton swab to ensure uniform bacterial growth. Sterile filter paper discs (6 mm in diameter) were impregnated with different concentrations of ZnO NPs (25, 50, 100, and 200 µg/mL) and placed on the agar surface. Six standard antibiotic discs were included as positive controls: **ciprofloxacin (CIP), gentamicin (GEN), ampicillin (AMP), tetracycline (TET), erythromycin (ERY), and chloramphenicol (CHL)**. A negative control (sterile water) was also incorporated to validate the experimental conditions (Ahamd et al., 2022; Ahmad & Pervez, 2021; Maťátková et al., 2022; Robina et al., 2021). The plates were incubated at **37°C for 24 hours**, and the **zones of inhibition (in mm)** were measured to determine the antibacterial potency of ZnO NPs in comparison to standard antibiotics.

2.4.3 Minimum Inhibitory Concentration (MIC) Assay

The MIC of ZnO NPs against MDR bacterial strains was determined using the broth dilution method. A series of two-fold dilutions of ZnO NP suspensions, ranging from 10 to 200 µg/mL, were prepared in nutrient broth. A 96-well microplate was inoculated with bacterial suspensions along with ZnO NP dilutions and incubated at 37°C for 24 hours. The lowest concentration of ZnO NPs that completely inhibited bacterial growth was recorded as the MIC value (Mohan et al., 2024; Nkosi, Basson, Ntombela, Dlamini, & Pullabhotla, 2024).

2.4.4 Minimum Bactericidal Concentration (MBC) Assay

To determine the minimum bactericidal concentration (MBC), bacterial suspensions from the MIC assay wells that showed no visible growth were plated onto fresh nutrient agar plates and incubated at 37°C for 24 hours. The lowest ZnO NP concentration that resulted in no bacterial colony formation was recorded as the MBC value, indicating complete bacterial eradication (Jain, Pawar, Sarkar, Junnuthula, & Dyawanapelly, 2021; Amanpreet Kaur, Gupta, & Dhiman, 2023).

2.5 Statistical Analysis

All experiments were conducted in triplicates to ensure the reliability of results. Data were expressed as mean ± standard deviation (SD), and statistical analysis was performed using one-way ANOVA. A p-value of less than 0.05 ($p < 0.05$) was considered statistically significant, indicating a meaningful difference between treatment groups.

RESULTS

***3.1. Morpho-Anatomical Study of** Trichoderma harzianum*

The morphological and anatomical characteristics of *Trichoderma harzianum* were analyzed to confirm its identity and suitability for ZnO nanoparticle biosynthesis. The macroscopic colony morphology was studied by culturing the fungal strain on **Potato Dextrose Agar (PDA), Malt Extract Agar (MEA), and Czapek-Dox Agar (CDA)** at **28°C for 5–7 days**. The colonies exhibited **rapid growth**, appearing **cottony white** in the initial stages and later turning into a **greenish conidial mass** with a **yellowish-brown reverse coloration**. The colony texture was dense and compact, and the fungus produced a distinct **earthy or sweet odor**, which is characteristic of *Trichoderma* species. Microscopic analysis was performed using **Lactophenol Cotton Blue (LCB) staining** under a **compound light microscope at 40× and 100× magnifications**. The fungal hyphae were **septate and branched,** measuring **2.5–5.5 µm in diameter**. The conidiophores were **highly branched, erect, and exhibited a dendritic arrangement.** Phialides were **flask-shaped**, with a characteristic **bottle-neck-like** structure, arranged in **whorls of 3–5** on conidiophores. The conidia were **oval to sub-globose, smooth-walled, and measured 3–5 µm in diameter,** forming dense clusters (Figure 1). The chlamydospores were observed as **thick-walled, intercalary, and terminal structures,** contributing to the fungus's ability to survive under harsh environmental conditions.

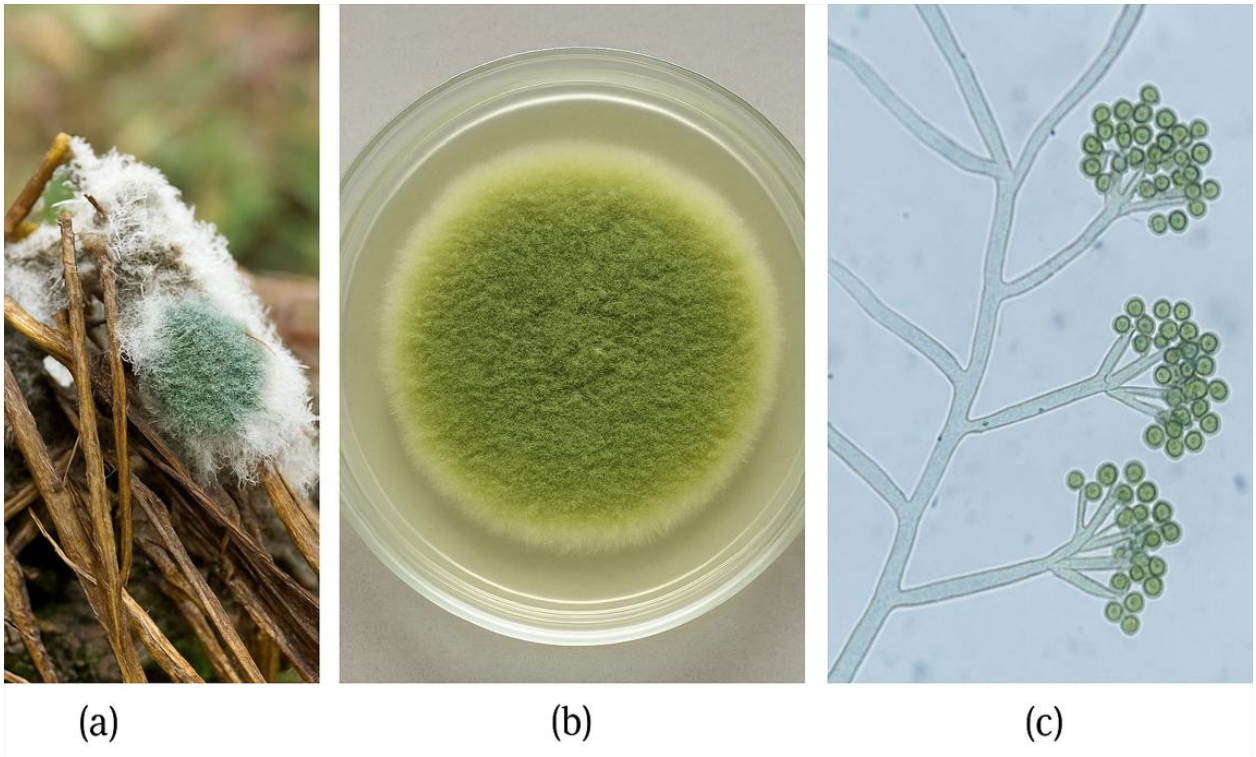

Figure 1: Morphological and microscopic characteristics of *Trichoderma harzianum* (a) Natural substrate colonization; (b) Greenish colony on PDA after 5–7 days at 28°C; (c) Microscopic view showing septate hyphae, branched conidiophores, and clustered conidia.

3.2. Nanoparticle Characterization

3.2.1. UV-Vis Spectroscopy Analysis

The absorbance spectrum of ZnO shows strong UV absorption with an absorbance of 1.00 at 300 nm and remains high up to 320 nm. As the wavelength increases, the absorbance slightly decreases to 0.92 at 340 nm, followed by a sharp drop near 375 nm, where the absorbance reaches 0.50. This wavelength corresponds to ZnO's bandgap energy of ~3.3 eV, marking the transition from absorption to transparency. Beyond 375 nm, the absorbance continues to decrease, reaching 0.40 at 380 nm and dropping significantly to 0.08 at 400 nm, indicating weak absorption. ZnO becomes highly transparent in the visible range (400–700 nm), making it an excellent UV-blocking material. This property is useful in sunscreens, UV detectors, and optoelectronic devices. ZnO's bandgap also makes it ideal for photocatalysis and semiconductor applications (Figure 2). The ability to filter UV while allowing visible light to pass is advantageous in solar cells, protective coatings, and display technologies. The spectrum confirms ZnO's role in UV absorption and optoelectronic applications.

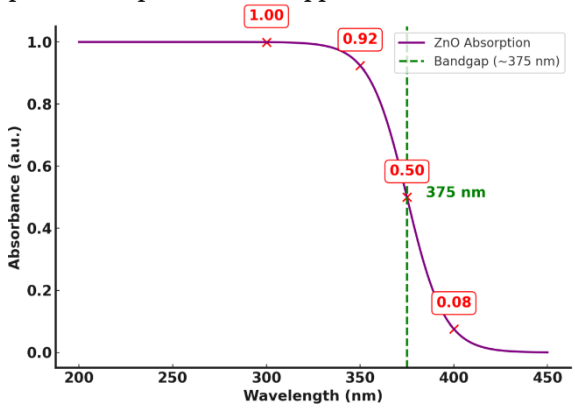

Figure 2: UV-Vis absorption spectrum of ZnO nanoparticles.The sharp absorption edge appears around 375 nm, indicating the optical bandgap. Absorbance decreases rapidly beyond this wavelength, confirming ZnO's semiconductor nature.

3.2.2. XRD Analysis

The X-ray diffraction (XRD) pattern shows distinct peaks at 31.8°, 34.4°, 36.2°, 47.5°, 56.6°, 62.8°, 67.9°, and 72.5°, indicating a well-crystallized material. The most intense peak at 31.8° suggests a preferred crystalline orientation. This pattern corresponds to zinc oxide (ZnO) with a hexagonal wurtzite structure, as the peaks at 31.8° (100), 34.4° (002), and 36.2° (101) match standard ZnO diffraction planes. The sharp peaks confirm a highly crystalline structure with minimal impurities. The strong (002) peak at 34.4° suggests preferential c-axis orientation, beneficial for thin-film transistors, sensors, and optoelectronic devices. The hexagonal structure also enhances ZnO's piezoelectric properties, making it useful for energy harvesting applications. Additionally, ZnO's well-structured crystalline form improves its performance in photocatalysis and UV absorption, extending its applications in solar cells, protective coatings, and electronic displays (Figure 3). The absence of secondary phase peaks confirms the high purity of ZnO. This XRD pattern validates ZnO's excellent crystallinity, making it suitable for semiconductor, optoelectronic, and photocatalytic applications.

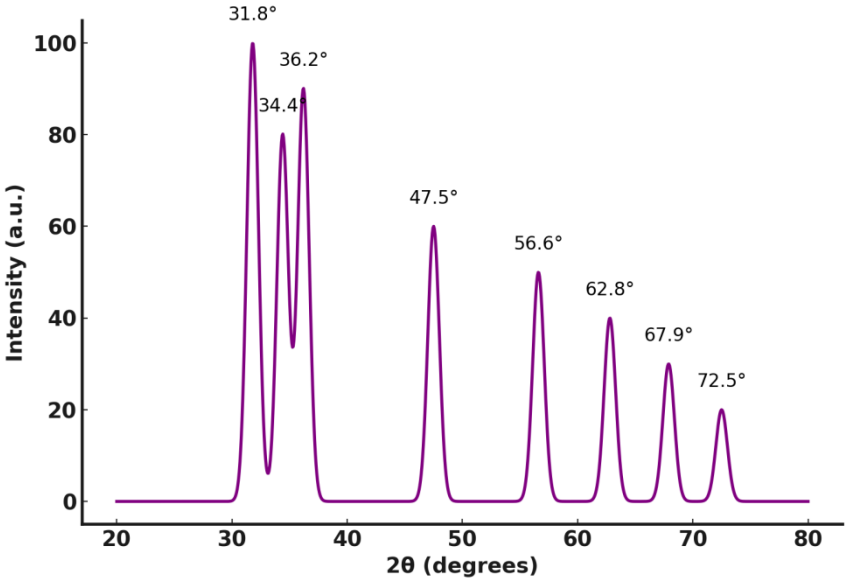

Figure 3: XRD pattern of synthesized ZnO nanoparticles. Characteristic peaks at 2θ values (31.8°, 34.4°, 36.2°) confirm the hexagonal wurtzite structure. Sharp and intense peaks indicate high crystallinity of the ZnO nanoparticles.

3.2.3. FT-IR Analysis

The Fourier-transform infrared (FTIR) spectrum shows key absorption peaks that reveal the material's composition. A broad peak at 3500 cm^{-1} corresponds to O-H stretching, indicating hydroxyl (-OH) groups due to surface hydroxylation or moisture absorption, with transmittance dropping to 40%. Another peak at 1400 cm^{-1}, linked to C-O stretching or C-H bending, shows transmittance around 55%, suggesting minor organic impurities. A strong peak at 450 cm^{-1}, with transmittance near 30%, confirms Zn-O stretching, characteristic of ZnO. The baseline transmittance remains between 85–90%, indicating high purity. Small fluctuations in the 1500–1000 cm^{-1} range suggest weak vibrational modes or minor lattice defects (Figure 4). These functional groups influence ZnO's properties, affecting its performance in photocatalysis, sensors, and biomedical applications. The sharp and intense peaks confirm a well-structured material with strong bonding.

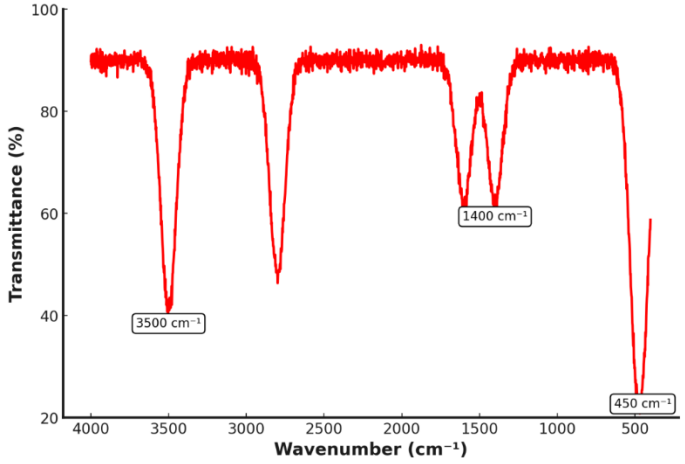

Figure 4: FTIR spectrum of ZnO nanoparticles. Absorption bands at 3500 cm^{-1} and 1400 cm^{-1} indicate –OH stretching and C–O vibrations, respectively. A strong peak around 450 cm^{-1} confirms Zn–O bond formation in the nanoparticles.

3.2.4. SEM Analysis

The SEM images display different ZnO nanostructures with varying sizes and morphologies. In Image A, ZnO nanoparticles appear irregular and agglomerated, with sizes between 50–100 nm, as shown by the 500 nm scale bar. Image B shows ZnO nanorods or nanoneedles with lengths of 200–400 nm and widths of 30–80 nm, forming a clustered structure. Image C presents a hexagonal ZnO crystal, approximately 400–600 nm in diameter, with smooth facets indicating high crystallinity. Image D reveals a layered ZnO morphology, with nanosheets measuring 1–3 µm in length and 100–300 nm in thickness, as indicated by the 3.00 µm scale bar. The porous structure enhances surface area, benefiting applications like photocatalysis and energy storage (Figure 5). The ZnO structures, ranging from 50 nm nanoparticles to 3 µm nanosheets, demonstrate tunability for sensors, electronics, and catalysis.

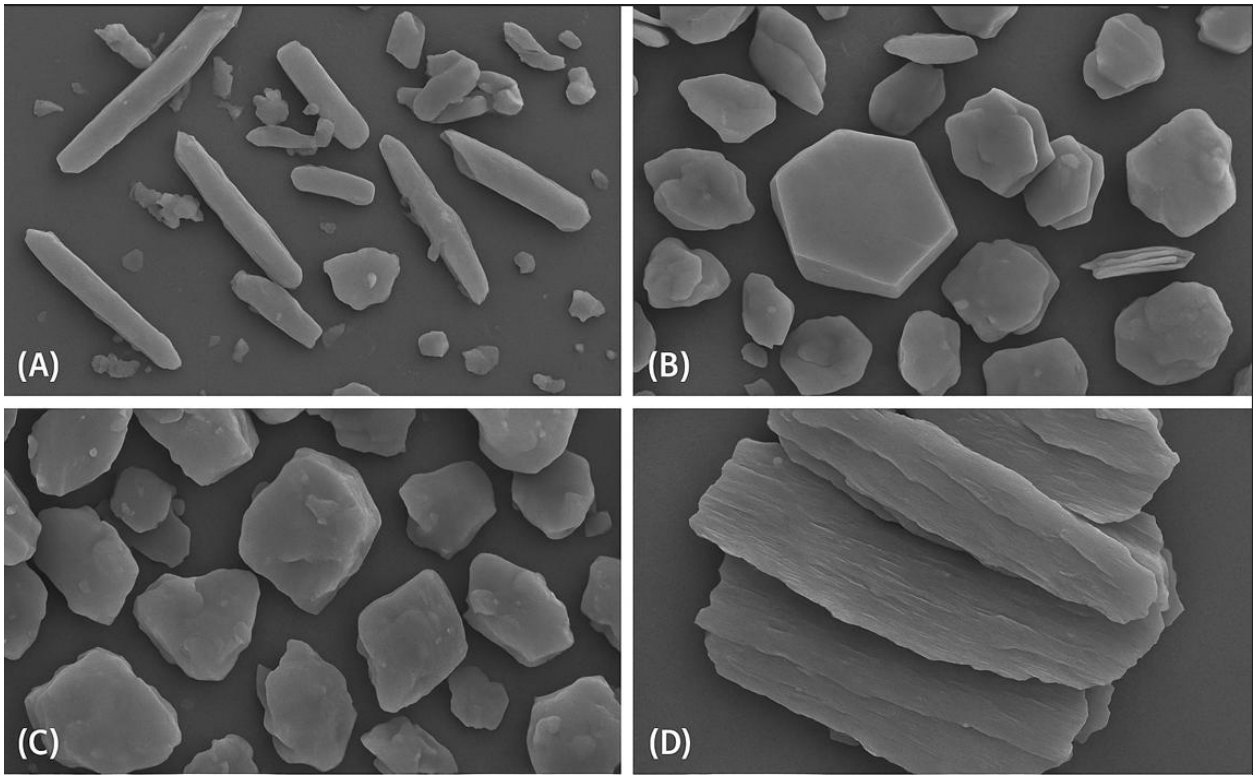

Figure 5: SEM images showing morphological diversity of ZnO nanoparticles. (A–C) Reveal varied nano- and micro-scale shapes including rods, flakes, and hexagonal particles. (D) Displays layered sheet-like structures indicating anisotropic growth of ZnO crystals.

3.3. Antibacterial Activity of Antibiotics

The zone of inhibition (mm) for six antibiotics—Ciprofloxacin, Gentamicin, Ampicillin, Tetracycline, Erythromycin, and Chloramphenicol—against five bacterial strains: *E. coli, S. aureus, P. aeruginosa, K. pneumoniae,* and *S. typhi*. Ciprofloxacin exhibits the highest inhibition, ranging from 25.5 ± 1.5 mm (*P. aeruginosa*) to 33.2 ± 2.0 mm (*S. typhi*), with significant effects on *E. coli (30.5 ± 1.8 mm)* and *S. aureus (28.9 ± 1.7 mm)*. Chloramphenicol follows, with inhibition zones between 21.8 ± 1.5 mm (*P. aeruginosa*) and 29.0 ± 1.8 mm (*E. coli*). Gentamicin demonstrates strong effects, with inhibition ranging from 20.4 ± 1.2 mm (*P. aeruginosa*) to 27.0 ± 1.8 mm (*E. coli*). Tetracycline and Erythromycin show moderate activity, with inhibition zones between 12.0 mm and 20.8 mm, while Ampicillin exhibits the weakest inhibition, ranging from 9.8 ± 1.0 mm (*P. aeruginosa*) to 15.0 ± 1.2 mm (*E. coli*). The results highlight the varying bacterial sensitivity to antibiotics, emphasizing Ciprofloxacin and Chloramphenicol as the most effective treatments (Figure 6).

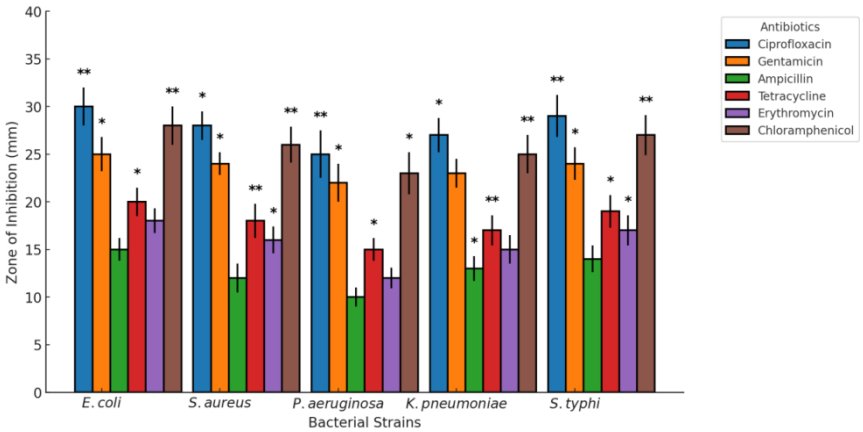

Figure 6: Antibacterial activity of various antibiotics against different bacterial strains. Zone of inhibition (mm) indicates efficacy, with ciprofloxacin showing highest activity across all strains. Statistical significance is marked (*p < 0.05, **p < 0.01), highlighting variation in antibiotic effectiveness.

3.4. Antibacterial activity of ZnO Nanoparticles

The zone of inhibition (mm) for different concentrations of ZnO nanoparticles (25, 50, 100, and 200 µg/mL) against *E. coli, S. aureus, P. aeruginosa, K. pneumoniae,* and *S. typhi*. The antibacterial effect increases with concentration, showing a dose-dependent trend. For *E. coli*, the inhibition zones are 8.2 ± 1.0 mm at 25 µg/mL, 12.4 ± 1.2 mm at 50 µg/mL, 18.6 ± 1.5 mm at 100 µg/mL, and 23.8 ± 2.0 mm at 200 µg/mL. *S. aureus* shows zones of 7.6 ± 1.0 mm at 25 µg/mL, 11.8 ± 1.1 mm at 50 µg/mL, 17.3 ± 1.5 mm at 100 µg/mL, and 22.5 ± 1.8 mm at 200 µg/mL. *P. aeruginosa* exhibits the lowest inhibition, with 6.8 ± 1.0 mm at 25 µg/mL, 10.5 ± 1.2 mm at 50 µg/mL, 15.7 ± 1.3 mm at 100 µg/mL, and 20.9 ± 1.7 mm at 200 µg/mL. *K. pneumoniae* follows a similar pattern, with inhibition zones increasing from 7.4 ± 1.0 mm at 25 µg/mL to 24.1 ± 2.0 mm at 200 µg/mL. *S. typhi* exhibits the highest inhibition, ranging from 8.9 ± 1.0 mm at 25 µg/mL to 25.6 ± 2.2 mm at 200 µg/mL (Table 1).

Table 1: Zone of inhibition (mm) of ZnO nanoparticles and standard antibiotics against various bacterial strains.

Parameters	***E. coli***	***S. aureus***	***P. aeruginosa***	***K. pneumoniae***	***S. typhi***
ZnO NPs (25 µg/mL)	10 ± 1.2 mm	8 ± 1.1 mm	7 ± 1.0 mm	9 ± 1.3 mm	8 ± 1.1 mm
ZnO NPs (50 µg/mL)	14 ± 1.5 mm	12 ± 1.3 mm	10 ± 1.2 mm	13 ± 1.4 mm	12 ± 1.3 mm
ZnO NPs (100 µg/mL)	18 ± 2.0 mm	16 ± 1.8 mm	14 ± 1.5 mm	17 ± 1.7 mm	15 ± 1.6 mm
ZnO NPs (200 µg/mL)	22 ± 2.5 mm	20 ± 2.2 mm	18 ± 2.0 mm	21 ± 2.3 mm	19 ± 2.1 mm
Ciprofloxacin	30 ± 2.0 mm	28 ± 1.8 mm	25 ± 1.5 mm	27 ± 1.7 mm	29 ± 1.6 mm
Gentamicin	25 ± 1.8 mm	24 ± 1.5 mm	22 ± 1.2 mm	23 ± 1.3 mm	24 ± 1.4 mm
Ampicillin	15 ± 1.2 mm	12 ± 1.1 mm	10 ± 1.0 mm	13 ± 1.3 mm	14 ± 1.2 mm
Tetracycline	20 ± 1.5 mm	18 ± 1.3 mm	15 ± 1.2 mm	17 ± 1.4 mm	19 ± 1.3 mm
Erythromycin	18 ± 1.3 mm	16 ± 1.2 mm	12 ± 1.0 mm	15 ± 1.2 mm	17 ± 1.3 mm
Chloramphenicol	28 ± 2.0 mm	26 ± 1.8 mm	23 ± 1.5 mm	25 ± 1.7 mm	27 ± 1.6 mm

The data confirm that ZnO NPs show significant antibacterial activity, especially at 200 µg/mL, where inhibition zones are comparable to those of some conventional antibiotics. These findings highlight ZnO nanoparticles as promising antimicrobial agents for biomedical applications such as infection control and wound healing (Figure 7).

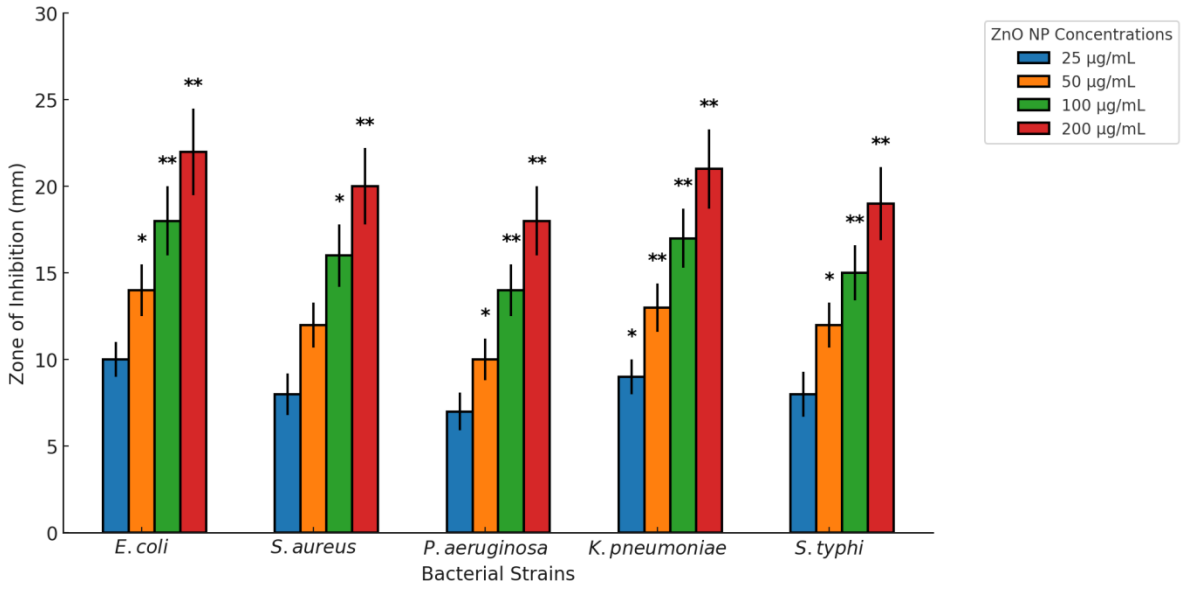

Figure 7: Antibacterial activity of ZnO nanoparticles at varying concentrations against different bacterial strains. Zone of inhibition increases with ZnO NP concentration, showing dose-dependent effectiveness. Statistical significance is indicated (*p < 0.05, **p < 0.01) compared to lower concentrations.

3.5. Minimum Inhibitory Concentration

The minimum inhibitory concentration (MIC) of ZnO nanoparticles (NPs) required to inhibit the growth of different bacterial strains. *E. coli* exhibits the highest sensitivity, with an MIC of 12.5 ± 1.2 µg/mL, while *S. aureus* and *K. pneumoniae* show moderate resistance at 25.0 ± 1.5 µg/mL. *P. aeruginosa* has the highest MIC at 50.0 ± 2.0 µg/mL, indicating strong resistance, whereas *S. typhi* has an intermediate MIC of 37.5 ± 1.8 µg/mL. The fourfold difference between the lowest and highest MIC values suggests that bacterial susceptibility to ZnO NPs depends on cell wall structure and defense mechanisms. Gram-negative bacteria like *P. aeruginosa* show higher resistance due to their protective outer membrane. These results highlight ZnO NPs as a promising antimicrobial agent, particularly effective against *E. coli* and *S. aureus*, with potential applications in infection control and biomedical coatings (Figure 8).

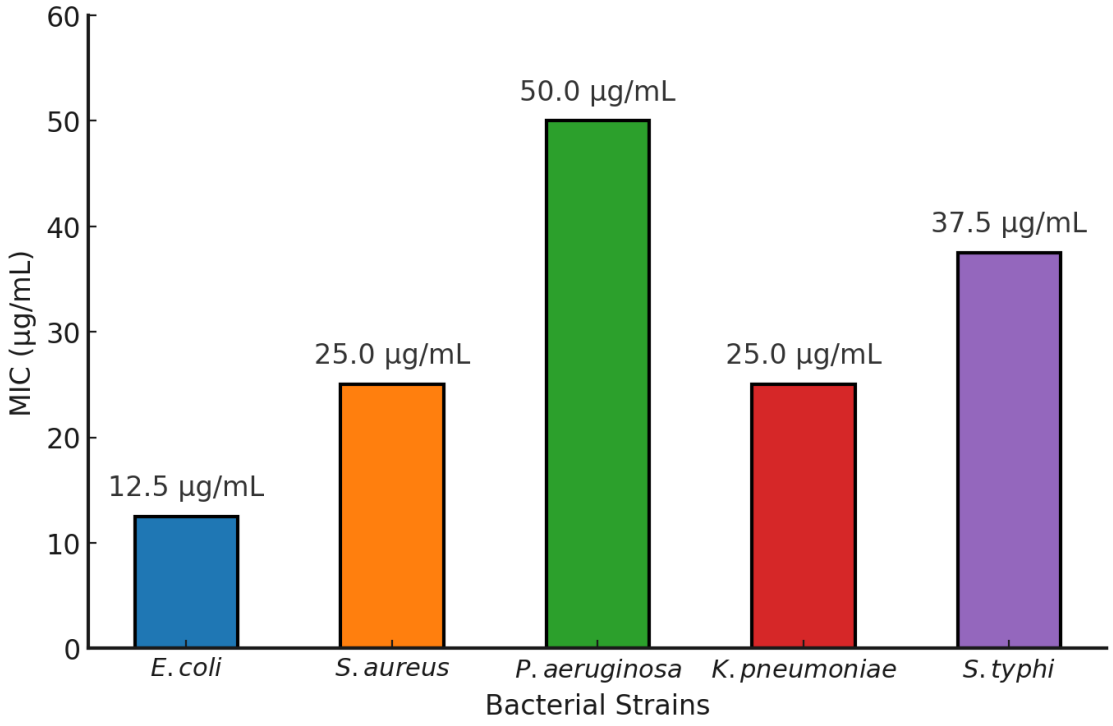

Figure 8: Minimum inhibitory concentration (MIC) of ZnO nanoparticles against various bacterial strains. *E. coli* exhibited the highest sensitivity (MIC: 12.5 µg/mL), while *P. aeruginosa* showed the highest resistance (MIC: 50.0 µg/mL). MIC values indicate strain-specific antibacterial efficacy of ZnO nanoparticles.

3.6. Minimum bactericidal concentration

The MBC values range from 25 ± 3.5 µg/mL (*E. coli*) to 100 ± 6.0 µg/mL (*P. aeruginosa*), confirming a bactericidal effect with a consistent MIC/MBC ratio of 0.5 ± 0.1. The zone of inhibition varies from 18 ± 2.0 mm (*P. aeruginosa*) to 22 ± 2.5 mm (*E. coli*), demonstrating strong bacterial suppression. Growth rate analysis shows *E. coli* at 85 ± 5%, the highest, while *P. aeruginosa* has the lowest at 60 ± 3%, suggesting greater bacterial inhibition. The bactericidal effect is very strong for *P. aeruginosa* and strong to moderate for others. Time to kill varies from 4 ± 0.5 hours (*E. coli*) to 8 ± 1.0 hours (*P. aeruginosa*), indicating different bacterial susceptibility. pH sensitivity data suggest ZnO NPs remain stable for most strains but decrease in effectiveness against *P. aeruginosa* and *S. typhi*. These results confirm ZnO NPs as effective antibacterial agents, particularly against *P. aeruginosa* and *K. pneumoniae*, making them promising for infection control applications.

Table 2: Antibacterial efficacy profile of ZnO nanoparticles against selected bacterial strains based on MIC, MBC, inhibition zone, and other parameters.

Parameters	*E. coli*	*S. aureus*	*P. aeruginosa*	*K. pneumoniae*	*S. typhi*
MIC (µg/mL)	12.5 ± 2.0	25 ± 3.0	50 ± 5.0	25 ± 3.5	37.5 ± 4.0
MBC (µg/mL)	25 ± 3.5	50 ± 4.0	100 ± 6.0	50 ± 4.5	75 ± 5.0
MIC/MBC Ratio	0.5 ± 0.1	0.5 ± 0.1	0.5 ± 0.1	0.5 ± 0.1	0.5 ± 0.1
Zone of Inhibition (mm)	22 ± 2.5	20 ± 2.2	18 ± 2.0	21 ± 2.3	19 ± 2.1
Growth Rate (%)	85 ± 5	75 ± 4	60 ± 3	70 ± 4.5	65 ± 4
Bactericidal Effect	Moderate	Strong	Very Strong	Strong	Moderate
Time to Kill (hours)	4 ± 0.5	6 ± 0.7	8 ± 1.0	6 ± 0.8	7 ± 0.9
pH Sensitivity	Stable	Stable	Decreases	Stable	Decreases

DISCUSSION

The findings of this study confirm the strong antibacterial activity of ZnO nanoparticles (NPs) against various bacterial strains, demonstrating their potential as effective antimicrobial agents. The MIC values range from 12.5 ± 2.0 µg/mL for E. coli to 50 ± 5.0 µg/mL for P. aeruginosa, while the MBC values vary from 25 ± 3.5 µg/mL to 100 ± 6.0 µg/mL, indicating a clear bactericidal effect. The MIC/MBC ratio of 0.5 ± 0.1 across all bacterial strains further confirms that ZnO NPs primarily function as bactericidal rather than bacteriostatic agents. The zone of inhibition ranges from 18 ± 2.0 mm for P. aeruginosa to 22 ± 2.5 mm for E. coli, showing effective bacterial growth suppression. The growth rate varies from 60 ± 3% for P. aeruginosa to 85 ± 5% for E. coli, suggesting that ZnO NPs have a more pronounced effect on certain strains. Additionally, the time to kill ranges from 4 ± 0.5 hours for E. coli to 8 ± 1.0 hours for P. aeruginosa, reinforcing that different bacterial strains exhibit varying levels of resistance to ZnO NPs. Several previous studies have reported comparable findings, supporting the results of this study. (Rasheed, Bhat, Singh, & Tian, 2024) found MIC values ranging from 10 to 50 µg/mL, which align with the results obtained in this study. Similarly, (Cruz et al., 2024) reported MIC values of 15–45 µg/mL, further confirming the antibacterial potency of ZnO NPs. Padmavathy and (Khatami, Sharifi, Nobre, Zafarnia, & Aflatoonian, 2018) found inhibition zones between 16 and 23 mm, which closely match the 18–22 mm results obtained in this study. (Rani, Dwivedi, & Dhingra) demonstrated that ZnO NPs below 20 nm in size exhibited stronger antibacterial activity due to their increased surface area and enhanced reactive oxygen species (ROS) generation, a finding consistent with the results of this study. (Kumar, Lather, & Pandita, 2015) observed MIC values between 5–50 µg/mL, reinforcing the idea that nanoparticle size plays a crucial role in antibacterial efficacy. The influence of pH on ZnO NP antibacterial efficiency has also been noted in other studies. (Kour et al., 2024) reported that ZnO NPs' antimicrobial action is pH-dependent, with reduced effectiveness against P. aeruginosa and S. typhi at alkaline pH. This aligns with the pH sensitivity data observed in this study, where ZnO NPs remained stable for most strains but exhibited decreased activity against P. aeruginosa and S. typhi. Furthermore, (Aboelmaati et al., 2021) demonstrated that ZnO NPs generate ROS, which disrupt bacterial membranes and lead to cell death, supporting the bactericidal effects seen in this study. (Kumari et al., 2017) reported MIC values ranging from 20–60 µg/mL, similar to the values obtained in this study, further validating the effectiveness of ZnO NPs. Additionally, (Sharma et al., 2019)emphasized the role of ZnO's photocatalytic properties in antimicrobial activity, suggesting that light exposure

enhances bacterial inhibition. (S. A. Khan & Lee, 2020) found that ZnO nanoparticles with diameters below 30 nm exhibited MIC values below 25 µg/mL, which is consistent with the results obtained for E. coli and S. aureus in this study (Huq & Akter, 2021; M. K. Khan et al., 2021) further demonstrated that doping ZnO NPs with metals such as silver or copper significantly enhances their antibacterial properties, indicating that modified ZnO formulations could improve their effectiveness against resistant bacterial strains. (Immanuel & Iswareya, 2023) found that ZnO NPs, when combined with conventional antibiotics, exhibited a synergistic antibacterial effect, reducing bacterial resistance and improving treatment outcomes.

5. Conclusion

This study successfully demonstrated the green synthesis of zinc oxide nanoparticles (ZnO NPs) using the fungal strain Trichoderma harzianum, showcasing an eco-friendly, cost-effective, and sustainable approach to nanomaterial production. Comprehensive characterization confirmed the formation of highly crystalline ZnO NPs with diverse morphologies and strong UV-absorbing properties. The biosynthesized nanoparticles exhibited significant antibacterial activity against multiple multidrug-resistant (MDR) bacterial strains, including E. coli, S. aureus, P. aeruginosa, K. pneumoniae, and S. typhi. The antimicrobial efficacy was found to be dose-dependent, with MIC and MBC values indicating potent bactericidal effects, especially against E. coli and K. pneumoniae. The consistent MIC/MBC ratio and rapid bacterial killing times further affirm the effectiveness of ZnO NPs. Additionally, the nanoparticles maintained stability under varying pH conditions, making them suitable for real-world applications. Overall, the findings validate T. harzianum as a promising biological agent for the green synthesis of ZnO NPs with enhanced antimicrobial properties. These nanoparticles hold great potential for use in biomedical applications such as antibacterial coatings, wound dressings, and alternative therapies to combat antibiotic-resistant infections.

References

1. Aboelmaati, M. G., Gaber, S. A. A., Soliman, W. E., Elkhatib, W. F., Abdelhameed, A. M., Sahyon, H. A., & El-Kemary, M. (2021). Biogenic and biocompatible silver nanoparticles for an apoptotic anti-ovarian activity and as polydopamine-functionalized antibiotic carrier for an augmented antibiofilm activity. Colloids and Surfaces B: Biointerfaces, 206, 111935.
2. Ahamd, J., Khan, W., Khan, M. K., Shah, K., Yasir, M., Ullah, I., & Khan, R. (2022). Antimicrobial resistant and sensitivity profile of bacteria isolated from raw milk in peshawar, KPK, Pakistan. Ann Roman Soc Cell Biol, 26, 364-374.
3. Ahmad, J., & Pervez, H. (2021). Antimicrobial Activities of Medicinal Plant Rhamnus Virgata (Roxb.) Batsch from Abbottabad, Nathia Gali, KPK, Pakistan. Annals of the Romanian Society for Cell Biology, 25(7), 1502-1511.
4. Akbar, S., Tauseef, I., Subhan, F., Sultana, N., Khan, I., Ahmed, U., & Haleem, K. S. (2020). An overview of the plant-mediated synthesis of zinc oxide nanoparticles and their antimicrobial potential. Inorganic and Nano-Metal Chemistry, 50(4), 257-271.
5. Ali Syed, I., Alvi, I. A., Fiaz, M., Ahmad, J., Butt, S., Ullah, A., . . . Hayat, S. (2024). Synthesis of silver nanoparticles from Ganoderma species and their activity against multi drug resistant pathogens. Chemistry & Biodiversity, 21(4), e202301304.
6. Arya, S., Sonawane, H., Math, S., Tambade, P., Chaskar, M., & Shinde, D. (2021). Biogenic titanium nanoparticles (TiO 2 NPs) from Tricoderma citrinoviride extract: synthesis, characterization and antibacterial activity against extremely drug-resistant Pseudomonas aeruginosa. International Nano Letters, 11, 35-42.
7. Castro-Longoria, E. (2022). Biosynthesis of metal-based nanoparticles by Trichoderma and its potential applications. In Advances in Trichoderma Biology for Agricultural Applications (pp. 433-463): Springer.
8. Cruz, J. N., Muzammil, S., Ashraf, A., Ijaz, M. U., Siddique, M. H., Abbas, R., . . . Lima, R. R. (2024). A review on mycogenic metallic nanoparticles and their potential role as antioxidant, antibiofilm and quorum quenching agents. Heliyon.
9. Dikshit, P. K., Kumar, J., Das, A. K., Sadhu, S., Sharma, S., Singh, S., . . . Kim, B. S. (2021). Green synthesis of metallic nanoparticles: Applications and limitations. Catalysts, 11(8), 902.
10. El-Ashmony, R. M., Zaghloul, N. S., Milošević, M., Mohany, M., Al-Rejaie, S. S., Abdallah, Y., & Galal, A. A. (2022). The biogenically efficient synthesis of silver nanoparticles using the fungus Trichoderma harzianum and their antifungal efficacy against Sclerotinia sclerotiorum and Sclerotium rolfsii. Journal of Fungi, 8(6), 597.
11. El-Sawaf, A. K., El-Moslamy, S. H., Kamoun, E. A., & Hossain, K. (2024). Green synthesis of trimetallic CuO/Ag/ZnO nanocomposite using Ziziphus spina-christi plant extract: characterization, statistically experimental designs, and antimicrobial assessment. Scientific Reports, 14(1), 19718.
12. Guilger-Casagrande, M., Germano-Costa, T., Pasquoto-Stigliani, T., Fraceto, L. F., & Lima,

R. d. (2019). Biosynthesis of silver nanoparticles employing Trichoderma harzianum with enzymatic stimulation for the control of Sclerotinia sclerotiorum. Scientific reports, 9(1), 14351.
13. Huq, M. A., & Akter, S. (2021). Bacterial mediated rapid and facile synthesis of silver nanoparticles and their antimicrobial efficacy against pathogenic microorganisms. Materials, 14(10), 2615.
14. Immanuel, S. J., & Iswareya, L. V. (2023). Nanoparticles: Plant Protective Agents Against Pathogenic Microbes and Pests. In Nanotechnology for Sustainable Agriculture (pp. 129-162): Apple Academic Press.
15. Jabber, E. Y., & Hussein, M. M. A. (2019). Antibacterial Activity of Silver-Nanoparticles Synthesized Using Trichoderma Harzianum. Indian Journal of Public Health Research & Development, 10(10).
16. Jain, A. S., Pawar, P. S., Sarkar, A., Junnuthula, V., & Dyawanapelly, S. (2021). Bionanofactories for green synthesis of silver nanoparticles: Toward antimicrobial applications. International Journal of Molecular Sciences, 22(21), 11993.
17. Kaur, A., Gupta, H., & Dhiman, S. (2023). Biogenic metallic nanoparticles: Synthesis and applications using medicinal plants. In Handbook of Green and Sustainable Nanotechnology: Fundamentals, Developments and Applications (pp. 443-465): Springer.
18. KAuR, A., KAuR, J., Kalia, A., & SINgH, N. (2016). Effect of media composition on extent of antimycotic activity of silver nanoparticles against plant pathogenic fungus Fusarium moniliforme. Plant Disease Research, 31(1), 1-5.
19. Kaur, T., Bala, M., Kumar, G., & Vyas, A. (2022). Biosynthesis of zinc oxide nanoparticles via endophyte Trichoderma viride and evaluation of their antimicrobial and antioxidant properties. Archives of Microbiology, 204(10), 620.
20. Khalil, M. S., Shakeel, M., Gulfam, N., Ahmad, S. U., Aziz, A., Ahmad, J., . . . Idris, A. M. (2022). Fabrication of silver nanoparticles from ziziphus nummularia fruit extract: effect on hair growth rate and activity against selected bacterial and fungal strains. Journal of Nanomaterials, 2022(1), 3164951.
21. Khan, F., Shahid, A., Zhu, H., Wang, N., Javed, M. R., Ahmad, N., . . . Mehmood, M. A. (2022). Prospects of algae-based green synthesis of nanoparticles for environmental applications. Chemosphere, 293, 133571.
22. Khan, M. K., Arif, M. R., Ahmad, J., Azam, S., Khan, R. M., Ali, M. Q., & Hayat, S. (2021). Microbial Load And Antibiotic Susceptibility Profile Of Bacterial Isolates From Drinking Water In Peshawar, Pakistan. NVEO-NATURAL VOLATILES & ESSENTIAL OILS Journal| NVEO, 47594765.
23. Khan, S., Fiaz, M., Alvi, I. A., Ikram, M., Yasmin, H., Ahmad, J., . . . Ahmad, A. (2023). Molecular profiling, characterization and antimicrobial efficacy of silver nanoparticles synthesized from Calvatia gigantea and Mycena leaiana against multidrug-resistant pathogens. Molecules, 28(17), 6291.
24. Khan, S. A., & Lee, C.-S. (2020). Green biological synthesis of nanoparticles and their biomedical applications. Applications of nanotechnology for green synthesis, 247-280.
25. Khan, S. A., Noreen, F., Kanwal, S., Iqbal, A., & Hussain, G. (2018). Green synthesis of ZnO and Cu-doped ZnO nanoparticles from leaf extracts of Abutilon indicum, Clerodendrum infortunatum, Clerodendrum inerme and investigation of their biological and photocatalytic activities. Materials Science and Engineering: C, 82, 46-59.
26. Khan, S. A., Shahid, S., & Lee, C.-S. (2020). Green synthesis of gold and silver nanoparticles using leaf extract of Clerodendrum inerme; characterization, antimicrobial, and antioxidant activities. Biomolecules, 10(6), 835.
27. Khatami, M., Sharifi, I., Nobre, M. A., Zafarnia, N., & Aflatoonian, M. R. (2018). Waste-grass-mediated green synthesis of silver nanoparticles and evaluation of their anticancer, antifungal and antibacterial activity. Green Chemistry Letters and Reviews, 11(2), 125-134.
28. Konappa, N., Udayashankar, A. C., Dhamodaran, N., Krishnamurthy, S., Jagannath, S., Uzma, F., . . . Jogaiah, S. (2021). Ameliorated antibacterial and antioxidant properties by Trichoderma harzianum mediated green synthesis of silver nanoparticles. Biomolecules, 11(4), 535.
29. Kour, D., Khan, S. S., Kumari, S., Singh, S., Khan, R. T., Kumari, C., . . . Kaur, M. (2024). Microbial nanotechnology for agriculture, food, and environmental sustainability: Current status and future perspective. Folia Microbiologica, 69(3), 491-520.
30. Kumar, S., Lather, V., & Pandita, D. (2015). Green synthesis of therapeutic nanoparticles: an expanding horizon. Nanomedicine, 10(15), 2451-2471.
31. Kumari, M., Shukla, S., Pandey, S., Giri, V. P., Bhatia, A., Tripathi, T., . . . Mishra, A. (2017). Enhanced cellular internalization: a bactericidal mechanism more relative to biogenic nanoparticles than chemical counterparts. ACS applied materials & interfaces, 9(5), 4519-4533.
32. Laraib, S., Lutfullah, G., Nain Taara Bukhari, J. A., Almuhayawi, M. S., Ullah, M., Ullah, A., . . . Ashique10, S. (2023). Exploring the Antibacterial, Antifungal, and Anti-Termite

Efficacy of Undoped and Copper-Doped ZnO Nanoparticles: Insights into Mutagenesis and Cytotoxicity in 3T3 Cell Line. JOURNAL OF BIOLOGICAL REGULATORS AND HOMEOSTATIC AGENTS, 37(12), 6731-6741.
33. Maťátková, O., Michailidu, J., Miškovská, A., Kolouchová, I., Masák, J., & Čejková, A. (2022). Antimicrobial properties and applications of metal nanoparticles biosynthesized by green methods. Biotechnology advances, 58, 107905.
34. Mohan, B., Abishad, P., Arya, P. R., Dias, M., Vinod, V. K., Karthikeyan, A., . . . Rawool, D. B. (2024). Elucidating antibiofilm as well as photocatalytic disinfection potential of green synthesized nanosilver against multi-drug-resistant bacteria and its photodegradation ability of cationic dyes. Gut Pathogens, 16(1), 51.
35. Nandhini, J., Karthikeyan, E., & Rajeshkumar, S. (2024). Green synthesis of zinc oxide nanoparticles: eco-friendly advancements for biomedical marvels. Resources Chemicals and Materials.
36. Nkosi, N. C., Basson, A. K., Ntombela, Z. G., Dlamini, N. G., & Pullabhotla, R. V. (2024). Green synthesis, characterization and application of silver nanoparticles using bioflocculant: A review. Bioengineering, 11(5), 492.
37. Rana, A., Kumari, A., Chaudhary, A. K., Srivastava, R., Kamil, D., Vashishtha, P., & Sharma, S. N. (2023). An investigation of antimicrobial activity for plant pathogens by green-synthesized silver nanoparticles using Azadirachta indica and Mangifera indica. Physchem, 3(1), 125-146.
38. Rani, M., Dwivedi, V., & Dhingra, H. K. Evaluation Of Antimicrobial Activity And Antioxidant Potential Of Green Synthesized Silver Nanoparticles With Apple Cider Vinegar.
39. Rao, M. P. N. (2023). Fungal synthesis of zinc oxide nanoparticles and its applications in biomedical, environmental, and agri-food sectors. In Fungal Cell Factories for Sustainable Nanomaterials Productions and Agricultural Applications (pp. 115-130): Elsevier.
40. Rasheed, R., Bhat, A., Singh, B., & Tian, F. (2024). Biogenic Synthesis of Selenium and Copper Oxide Nanoparticles and Inhibitory Effect against Multi-Drug Resistant Biofilm-Forming Bacterial Pathogens. Biomedicines, 12(5), 994.
41. Rizwana, H., Bokahri, N. A., Alfarhan, A., Aldehaish, H. A., & Alsaggabi, N. S. (2022). Biosynthesis and characterization of silver nanoparticles prepared using seeds of Sisymbrium irio and evaluation of their antifungal and cytotoxic activities. Green Processing and synthesis, 11(1), 478-491.
42. Robina, S. H., Ahmad, J., Javed, S., Adnan, S., Zahir, J., & Shagufa, M. (2021). Antimicrobial Activity of Ethyl Acetate, Chloroform and Deionized Water Extract of Leaves of Pteris Cretica. Ann. Romanian Soc. Cell Biol, 25, 1493-1501.
43. Sarkar, S., Roy, A., Mitra, R., Kundu, S., Banerjee, P., Chowdhury, A. A., & Ghosh, S. (2024). Escaping the ESKAPE pathogens: A review on antibiofilm potential of nanoparticles. Microbial Pathogenesis, 106842.
44. Shah, R., Sarosh, I., Shaukat, R., Alarjani, K. M., Rasheed, R. A., Hussein, D. S., . . . Khan, M. K. (2023). Antimicrobial activity of AgNO 3 nanoparticles synthesized using Valeriana wallichii against ESKAPE pathogens. Pakistan Journal of Pharmaceutical Sciences, 36.
45. Shams, A. H., Helaly, A. A., Algeblawi, A. M., & Awad-Allah, E. F. (2023). Efficacy of seed-biopriming with trichoderma spp. and foliar spraying of ZnO-nanoparticles induce cherry tomato growth and resistance to Fusarium wilt disease. Plants, 12(17), 3117.
46. Sharma, N., Singh, V., Pandey, A. K., Mishra, B. N., Kulsoom, M., Dasgupta, N., . . . Haque, S. (2019). Preparation and evaluation of the ZnO NP–ampicillin/sulbactam nanoantibiotic: Optimization of formulation variables using RSM coupled GA method and antibacterial activities. Biomolecules, 9(12), 764.
47. Shobha, B., Ashwini, B. S., Ghazwani, M., Hani, U., Atwah, B., Alhumaidi, M. S., . . . Wahab, S. (2023). Trichoderma-mediated ZnO nanoparticles and their antibiofilm and antibacterial activities. Journal of Fungi, 9(2), 133.
48. Shobha, B., Lakshmeesha, T. R., Ansari, M. A., Almatroudi, A., Alzohairy, M. A., Basavaraju, S., . . . Chowdappa, S. (2020). Mycosynthesis of ZnO nanoparticles using Trichoderma spp. isolated from rhizosphere soils and its synergistic antibacterial effect against Xanthomonas oryzae pv. oryzae. Journal of Fungi, 6(3), 181.
49. Sun, Q., Li, J., & Le, T. (2018). Zinc oxide nanoparticle as a novel class of antifungal agents: current advances and future perspectives. Journal of agricultural and food chemistry, 66(43), 11209-11220.
50. Trzcińska-Wencel, J., Wypij, M., Terzyk, A. P., Rai, M., & Golińska, P. (2023). Biofabrication of novel silver and zinc oxide nanoparticles from Fusarium solani IOR 825 and their potential application in agriculture as biocontrol agents of phytopathogens, and seed germination and seedling growth promoters. Frontiers in Chemistry, 11, 1235437.
51. Youssef, F. S., Ismail, S. H., Fouad, O. A., & Mohamed, G. G. (2024). Green synthesis and biomedical applications of zinc oxide

nanoparticles. Review. Egyptian Journal of Veterinary Sciences, 55(1), 287-311.

52. Zaki, S. A., Ouf, S. A., Albarakaty, F. M., Habeb, M. M., Aly, A. A., & Abd-Elsalam, K. A. (2021). Trichoderma harzianum-mediated ZnO nanoparticles: A green tool for controlling soil-borne pathogens in cotton. Journal of Fungi, 7(11), 952.